Optimization of a three-dimensional hybrid system combining a floating breakwater and a wave energy converter array

Hengming Zhang[a], Binzhen Zhou[b*], Jun Zang[c], Christopher Vogel[d], Peng Jin[a], Dezhi Ning[e]

[a]*College of Shipbuilding Engineering, Harbin Engineering University, Harbin 150001, China*

[b]*School of Civil Engineering and Transportation, South China University of Technology, Guangzhou 510641, China*

[c]*Department of Architecture and Civil Engineering, University of Bath, Bath, BA2 7AY, United Kingdom*

[d]*Department of Engineering Science, University of Oxford, OX1 3PJ, United Kingdom*

[e]*State Key Laboratory of Coastal and Offshore Engineering, Dalian University of Technology, Dalian 116023, China*

Abstract

Combining wave energy converters (WECs) with a floating breakwater provides a potential approach to help develop commercial-scale wave power operations. This paper aims to design and optimize a three-dimensional floating breakwater integrated with a WEC array by developing a numerical model of a multi-floating-body coupled system based on potential flow theory with viscous correction in the frequency domain. By analyzing the wave surface elevations around the breakwater, the size of the breakwater was optimized and the optimal installation locations of the WECs were determined. Under the condition of coupled constraints and six degrees-of-freedom motion, the interactions between the WEC array and the breakwater were analyzed. Subsequently, the number of WECs and the distance between the WECs and the breakwater were optimized to maximize the wave energy conversion performance of the hybrid system. Results show that the wave focusing areas appear more frequently near the breakwater. These focusing areas significantly improve WEC power, and thus better wave energy conversion performance can be achieved when the WECs is placed close to the breakwater. The vertical forces on the breakwater significantly increase due to the presence of the WECs, however the horizontal forces are decreased. The findings of this paper provide guidance to design and optimize a hybrid WEC-breakwater system in practical engineering applications.

Key Words: Wave energy converter; Floating breakwater; Multi-floating-body; Coupled constraint motion; Wave attenuation; Wave focusing.

1 Introduction

The high costs and low energy extraction performance of Wave Energy Converters (WECs) make the electricity generated by WECs less competitive compared with the conventional generation technologies (e.g., gas, coal) and other renewable energies (e.g. solar photovoltaic, wind energy) [1]. Integrating WECs with other offshore structures has been introduced by Mustapa et al. [2] and Zhao et al. [3] as a method for making wave power operations more feasible through improved wave extraction performance, cost-sharing, space-sharing and multi-functionality of devices. Examples include Oscillating Water Columns (OWC) integrated with breakwaters [4] [5], Oscillating Buoys (OB) integrated with floating breakwaters [6], integration of an OWC with an offshore wind turbine monopile [7], and integration of different type WECs [8]. The OWC integrating with breakwater has been widely studied by researchers,

* Corresponding author
E-mail address: zhoubinzhen@scut.edu.cn (B.Z. Zhou)

such as He et al. [9] [10], Zheng & Zhang [11], and Xu & Huang [12].

Another widely studied integrated system is a floating breakwater combined with an OB type WEC because of the reduced dependence on seabed conditions and the superior energy conversion efficiency that can be achieved. Integration of the breakwater and WEC can take different forms, with a principal distinction being between single-floaters, wherein WEC power take-off is added to the floating breakwater, and dual-floaters, where the WEC is deployed in front of, and moves relative to the floating breakwater. Zhang et al. [13] found a single-floater integrated system with an asymmetric bottom had higher power conversion efficiency and better wave attenuation performance than that with symmetric bottom, with the maximum conversion efficiency over 92% at the resonant frequency. Other researchers also have studied the single-floater integrated system, such as Madhi et al. [14], Ning & Zhao [15], Zhao et al. [16], and Chen & Zang [17]. However, the conversion efficiency of the single-floating integrated system is lower at non-resonant frequencies, especially in the low-frequency region, resulting in a smaller effective frequency range. Placing a floating breakwater behind the WEC can improve the conversion efficiency of the WEC in the low frequency region. Zhao & Ning [18] experimentally studied a novel two-pontoon system consisting of a front OB-type WEC and a rear fixed pontoon, demonstrating that the wave energy extraction performance of the two-pontoon system was significantly better than that of the single-pontoon system without reducing the wave attenuation performance. Ning et al. analytically [19] and experimentally [20] studied the performance of a dual-pontoon floating breakwater that also acted as a WEC and they found that the dual pontoon-PTO system broadened the effective frequency range compared with a single pontoon-PTO system with the same pontoon volume. Similar conclusions were drawn by Zhang et al. [21] [22], who compared the wave extraction and wave attenuation performance of a dual-floater WEC-breakwater hybrid system with those of the corresponding single-floater integrated system and investigated the wave resonance [23] in the WEC-breakwater gap using CFD software Star-CCM+. The maximum conversion efficiency of the hybrid system with a symmetric WEC reaches 61%, which is higher than the theoretical maximum conversion efficiency of 50% for a symmetric heaving device. In practice, the hybrid WEC-breakwater system is three-dimensional and contains multiple WECs, which introduces some three-dimensional problems. For example, the motion of a WEC could influence the hydrodynamic coefficients of other WECs, which in turn affects the wave extraction performance of the WECs. Therefore, it is essential to develop three-dimensional models to study the performance of the hybrid WEC-breakwater system, which can provide useful insights into practical applications of WECs and floating breakwaters.

Only a few investigations to date have concentrated on the three-dimensional dynamics of hybrid WEC-breakwater systems. Ning et al. [24] studied the performance of a WEC array integrated with a pontoon-type breakwater based on the linear potential flow theory. They showed that the energy conversion efficiency of a WEC array with a pontoon is much higher than that without a pontoon. The same integrated system comprising of a WEC array and a fixed breakwater was studied experimentally by Zhao et al. [25] and similar conclusions were drawn. Cheng et al. [26] performed an analysis of the performance and the design of a moonpool-type floating breakwater combined with an OB-type WEC array. They found the energy extraction performance of the WECs was promoted by the internal fluid motion in the moonpools, which in turn enhanced the wave attenuation capacity of the floating breakwater. These previous works assumed the breakwater to be fixed and only considered single degree-of-freedom (DoF) motion of the WEC.

However, floating breakwaters are secured by a mooring system in practice and thus the motion of the floating breakwaters is 6-DoF, which has yet to be investigated.

In practical engineering applications, the WEC array could be installed on the breakwater to make the mooring system of the WECs unnecessary, which is conducive to reducing the cost of the hybrid WEC-breakwater system. Installing the WECs on a breakwater introduces new challenges of multi-floating-body coupled constraints motion. Some research has been carried out on dual-floater coupled constraints motion [27]. Sun et al. [28] investigated the wave-induced responses of constrained multiple bodies based on linear diffraction theory. Ruehl et al. [29] simulated the heave, pitch, and surge motions of a RM3 WEC using the open-source WEC-Sim software. Based on the three-dimensional wave radiation-diffraction method, Zheng et al. [30] carried out a dynamic analysis of a two-raft wave energy conversion device consisting of two hinged cylindrical rafts and a power take-off system at the joint. Zheng & Zhang [31] analytically investigated the wave power capture capacity of two interconnected floats with arbitrary float length, showing that with the forward float shorter than the aft one achieves higher power absorption. Zhang et al. [32] investigated the maximum wave energy conversion by a hinged flexible two-floater WEC, which indicated that the structural flexibility had a negative effect on the power capture performance for relatively large wave length but a positive influence for relatively small wave length. Relatively few studies have been carried out for multi-floating-body coupled constraints motion. Sricharan & Chandrasekaran [33] conducted a detailed numerical analysis of a system consisting of a set of WECs connected to a central buoy using WEC-Sim. To the best of authors' knowledge, the technology to solve the dual- or multi-floating-body coupled constraints motion has not been expanded to simulate the cases of multi-floating-body coupled constraints motion of the hybrid WEC-breakwater system with 6-DoF, which needs further investigation.

Previous studies on OB-type WECs integrated with a breakwater mainly focused on the interactions between WECs, and WECs and the breakwater, which cannot provide an efficient method to design and optimize a hybrid WEC-breakwater system in a specific sea state for practical engineering purposes. Ren et al. [34] provided a way to determine the wave attenuation and focusing performance of a breakwater with different geometric factors simultaneously by analyzing the wave elevations in the deployment and protection zones, so as to optimize the size of the breakwater. Other researchers have also investigated wave elevations around the breakwater. Duan et al. [35] analytically studied the sheltering effects on an arc-shaped floating perforated breakwater and Chu et al. [36] studied the effects of incident wave parameters and structural configurations on the hydrodynamic force and wave elevation in wave field of an arc-shaped bottom-mounted breakwater. Chang et al. [37] investigated the wave height distribution around a V-shaped breakwater with different incident wave angles. Moreover, the effects of varying dimensions of the WEC, mooring stiffness, wave periods and wave directions on the wave extraction and coastal protection performance of a multiple-raft WEC integrated with a floating breakwater were studied by Tay [38], and the wave elevations surrounding the integrated system were also shown. These distribution maps of wave amplitude around the breakwater in previous studies clearly showed the positions of wave focusing areas, which can be used as a basis for quickly predicting the optimal placement of the WECs but are usually neglected by researchers. Therefore, this paper verified the feasibility of determining the optimal position through distribution maps of wave elevations around a breakwater.

Existing studies can only provide limited references for practical design of the hybrid WEC-breakwater system. This study aims to design and optimize the layout of the WEC-breakwater hybrid system based on field conditions to provide a reference for practical application in engineering. The novelties and motivations of the present work are fourfold. Firstly, to establish a numerical model with viscous correction [39] to describe the interactions between waves and a multi-floating-body connected by constraints. Secondly, to design the configuration of the breakwater by analyzing the distribution of wave amplitude around the breakwater and to investigate the wave extraction performance of the WECs with the hybrid system subject to 6-DoF including the influence of moorings, which is closer to real situations. Thirdly, to evaluate the wave attenuation performance and locate the areas with better wave focusing based on an annual field data of wave conditions. Finally, to optimize the layout of the WEC and the array deployment based on the findings obtained by analyzing the distribution of the wave amplitude around the breakwater.

The paper is structured as follows. In Section 2, the numerical model of the hybrid WEC-breakwater system is briefly introduced. In Section 3, the numerical model is verified through comparison to published WEC-Sim results. In Section 4, the design and optimization of the hybrid WEC-breakwater system, including the size of the breakwater, the layout and number of the WECs, and the distance between the WECs and breakwater, are carried out. Finally, conclusions are drawn in Section 5.

2 Numerical models

2.1 Hybrid WEC-breakwater system

Fig. 1 shows the sketch of the proposed hybrid WEC-breakwater system. The hybrid WEC-breakwater system consists of a floating breakwater, wave energy converter arrays, and a mooring system. The tensioned mooring lines are connected to the bottom of the breakwater and the seabed. Thus the motion of the floating breakwaters is 6-DoF. The definition of motion mode and sign of the hybrid WEC-breakwater system are shown in Fig. 2. The mooring system was represented by the equivalent stiffness matrix calculated from the deformation and elastic modulus of the mooring line.

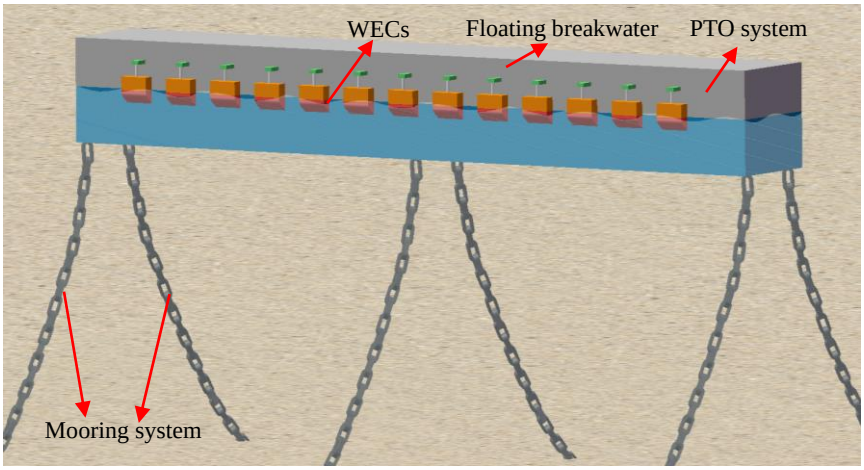

Fig. 1 Sketch of the hybrid WEC-breakwater system

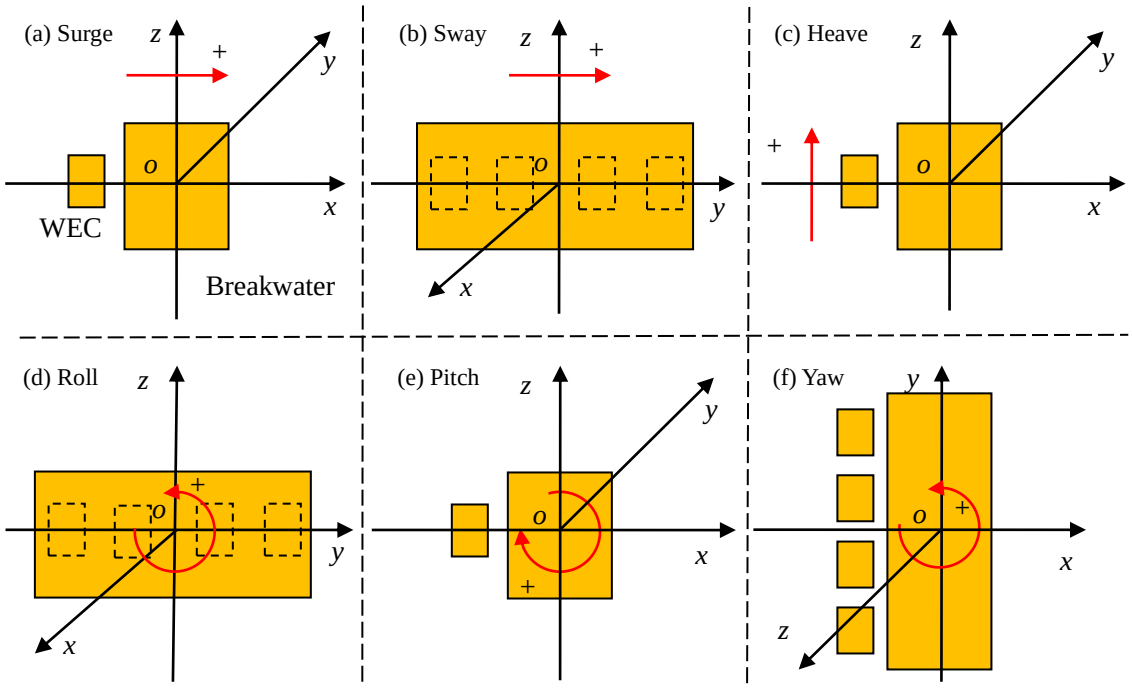

Fig. 2 Definition sketch of motion mode and sign

The corresponding side view and plan view of the hybrid WEC-breakwater system are shown in Fig. 3 The WECs were connected to the floating breakwater through the PTO system and can move in heave mode relative to the floating breakwater. But in the other five DoF, the WECs were restricted to move with the breakwater, i.e. stationary relative to the breakwater. The length of the breakwater L=150.0 m, the water depth h=60.0 m, water density was ρ = 1023 kg/m^3 and the incident wave amplitude A_i=1.0 m were considered for all the cases in Section 4. The transmission wave amplitude A_t was measured by the average surface elevations of a measurement area on the lee side and the focusing wave amplitude A_f was obtained by the average surface elevations of the focusing areas where wave amplitude A_f >2.0 m [34] in a measurement area on the upward side of the breakwater, as shown in Fig. 3 (b). The size of the measurement area was chosen as 50.0 m×L according to Ref [34], and the results obtained by a 100.0 m×L area are very close to that by a 50.0 m×L area. To reduce the calculation time, 50.0 m×L was chosen as the size of the measurement area. Table 1 shows the joint distribution S_j of average wave height H_j and wave period T_j for one year in the sea area around an island in the South China Sea, which was used as a reference for system evaluation in this paper. The water depth of this sea area is h=60.0 m.

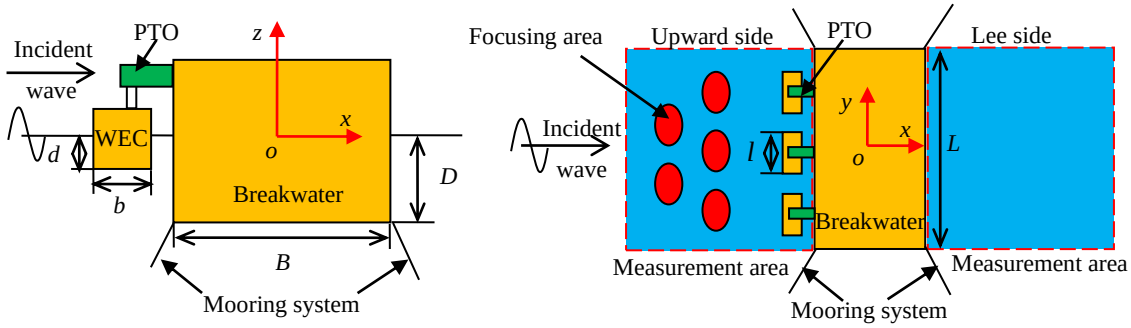

(a) Side view (b) Plan view

Fig. 3 Side view (a) and plan view (b) of the hybrid WEC-breakwater system

Table 1 Joint distribution S_j of wave height H_j and wave period T_j for one year in the sea area around an island in the South China Sea (Unit: %)

H_j \ T_j	1.0-2.0	2.0-3.0	3.0-4.0	4.0-5.0	5.0-6.0	6.0-7.0	7.0-8.0	8.0-9.0
0-0.5	0.007	2.171	4.506	1.831	0.945	0.038	0	0
0.5-1.0	0	0.021	7.347	13.590	6.734	3.892	0.938	0.014
1.0-1.5	0	0	0.003	4.345	11.567	4.701	2.756	1.102
1.5-2.0	0	0	0	0.007	2.420	7.946	1.852	0.582
2.0-2.5	0	0	0	0	0.021	3.888	4.546	0.418
2.5-3.0	0	0	0	0	0	0.133	5.357	1.078
3.0-3.5	0	0	0	0	0	0	0.774	2.896
3.5-4.0	0	0	0	0	0	0	0.014	1.418
4.0-4.5	0	0	0	0	0	0	0	0.133
Total	0.007	2.192	11.856	19.782	21.687	20.598	16.237	7.641

2.2 Motion equation of floaters

For the hybrid WEC-breakwater system with n WECs and one breakwater, the motion equation can be written as [28]

$$\begin{bmatrix} \boldsymbol{L}_{6(n+1)\times 6(n+1)} & \boldsymbol{D}^{T}_{6(n+1)\times 5n} \\ \boldsymbol{D}_{5n\times 6(n+1)} & \boldsymbol{0}_{5n\times 5n} \end{bmatrix} \begin{bmatrix} \boldsymbol{\xi}_{6(n+1)\times 1} \\ \boldsymbol{f}_{L,5n\times 1} \end{bmatrix} = \begin{bmatrix} \boldsymbol{f}_{ex,6(n+1)\times 1} \\ \boldsymbol{0}_{5n\times 1} \end{bmatrix} \tag{1}$$

where $[\boldsymbol{L}]=-\omega^2([\boldsymbol{M}]+[\boldsymbol{a}])-\mathrm{i}\omega^2([\boldsymbol{b}]+[\boldsymbol{b}_{\mathrm{vis}}]+[\boldsymbol{b}_{\mathrm{PTO}}])+[\boldsymbol{C}]+[\boldsymbol{k}_{\mathrm{stiff}}]+[\boldsymbol{k}_{\mathrm{PTO}}]$, ω is wave frequency and i is the imaginary unit. $[\boldsymbol{M}]$ and $[\boldsymbol{C}]$ are the rigid body mass matrix and the restoring force matrix respectively for $n+1$ floaters. $[\boldsymbol{b}_{\mathrm{PTO}}]$ and $[\boldsymbol{k}_{\mathrm{PTO}}]$ represent the mechanical damping and stiffness matrices of the PTO system respectively. $[\boldsymbol{k}_{\mathrm{stiff}}]$ corresponds to the stiffness matrix of the mooring system and $[\boldsymbol{b}_{\mathrm{vis}}]$ is the viscous damping matrix. The added mass matrix $[\boldsymbol{a}]$, radiation damping matrix $[\boldsymbol{b}]$, and exciting forces and moments matrix $[\boldsymbol{f}_{\mathrm{ex},\ 6(n+1)\times 1}]$ are calculated using the code package WAFDUT [40] based on the linear frequency domain potential flow theory and higher-order boundary element method. $[\boldsymbol{\zeta}_{6(n+1)\times 1}]$ is the motion matrix of the floaters, $[\boldsymbol{D}_{5n\times 6(n+1)}]$ is the constraint matrix [28] and $[\boldsymbol{f}_{\mathrm{L},5n\times 1}]$ is the force and moment generated by the connection between the WECs and the breakwater. $[\boldsymbol{D}_{5n\times 6(n+1)}]$ can be expressed as [28]

$$\boldsymbol{D}_{5n\times 6(n+1)} = \begin{bmatrix} D_1^1 & 0 & 0 & 0 & 0 & D_{n+1}^1 \\ 0 & \ddots & 0 & 0 & 0 & \vdots \\ 0 & 0 & D_i^i & 0 & 0 & D_{n+1}^i \\ 0 & 0 & 0 & \ddots & 0 & \vdots \\ 0 & 0 & 0 & 0 & D_n^n & D_{n+1}^n \end{bmatrix} \tag{2}$$

where

$$D_i^i = \begin{bmatrix} 1 & 0 & 0 & 0 & z_i - z_{ci} & -(y_i - y_{ci}) \\ 0 & 1 & 0 & -(z_i - z_{ci}) & 0 & x_i - x_{ci} \\ 0 & 0 & 0 & 1 & 0 & 0 \\ 0 & 0 & 0 & 0 & 1 & 0 \\ 0 & 0 & 0 & 0 & 0 & 1 \end{bmatrix} \quad (i=1,\ n) \tag{3}$$

$$D_{n+1}^{i}=\begin{bmatrix} -1 & 0 & 0 & 0 & -(z_i - z_{c(n+1)}) & y_i - y_{c(n+1)} \\ 0 & -1 & 0 & z_i - z_{c(n+1)} & 0 & -(x_i - x_{c(n+1)}) \\ 0 & 0 & 0 & -1 & 0 & 0 \\ 0 & 0 & 0 & 0 & -1 & 0 \\ 0 & 0 & 0 & 0 & 0 & -1 \end{bmatrix} \quad (i=1, n) \tag{4}$$

where (x_i, y_i, z_i) and (x_{ci}, y_{ci}, z_{ci}) are the point at which they are connected and the global coordinates of the rotation centres of each floater respectively. Thus, according to Eq.(1), we can obtain the motions of the WECs and breakwater.

2.3 Wave power of WECs and distribution of surface elevations

The total wave power P_{total} (T) and the total wave power per unit mass P_{ave} (T) of the WEC array at wave period T are defined as

$$P_{total}(T)=\sum_{i=-(n-1)/2}^{(n-1)/2} P_i(T) \tag{5}$$

$$P_{ave}(T)=\frac{P_{total}(T)}{m_{total}} \tag{6}$$

where m_{total} is the total mass of the WEC array and n is the total number of WECs. P_i (T) is the wave power produced by the WEC numbered i at wave period T with the incident wave amplitude A_i=1.0 m, which is defined as

$$P_i(T)=\frac{1}{2}(\frac{2\pi}{T})^2 b_{opt}\left|\zeta_{3i}\right|^2 \tag{7}$$

where b_{opt} is the optimal damping of the PTO system, which is calculated through numerical optimization (see [41] for further details). ζ_{3i} corresponds to the heave motion of the WEC numbered i.

The total Annual Energy Production (AEP) W_{AEP} and the total AEP per unit mass $W_{AEP/mass}$ of the WEC array are defined as

$$W_{AEP}=\sum_{i=-(n-1)/2}^{(n-1)/2} W_{AEP\text{-}i} \tag{8}$$

$$W_{AEP/mass}=\frac{W_{AEP}}{m_{total}} \tag{9}$$

where $W_{AEP\text{-}i}$ is AEP produced by the WEC numbered i in one year, which is defined as

$$W_{AEP\text{-}i}=\sum_{j=1}^{N}[(\frac{H_j}{2})^2 \times P_i(T_j)\times S_j]\times t_{year} \tag{10}$$

where T_j, H_j, and S_j are the wave period, the wave height, and the probability of the j th wave component in Table 1. N is the total number of wave components in Table 1. t_{year} is the total times of one year.

The complex surface elevation η can be expressed as [42]

$$h=(\frac{j_{D}}{ig/w}+K\sum_{k=1}^{6} z_k j_{rk})_{z=0} \tag{11}$$

where φ_D, ζ_k ,and φ_{rk} are the diffraction potentials, the motion response, and the radiation potential in k th mode oscillating with unit amplitude respectively, which are calculated by the code package WAFDUT [40]; K is the wave number; g is the acceleration of gravity.

3 Verification

To validate the present numerical model, a RM3 WEC [29] was simulated in this section. The

dimensions and mass properties of the RM3 WEC are shown in Fig. 4 and Table 2. The water depth was h = 49.5 m and the water density was ρ = 1000 kg/m^3. The incident wave height was H_i=2.5 m.

The motion of the RM3 WEC has been calculated by Ruehl et al. [29] using WEC-Sim code. The code is a time-domain modeling tool developed in MATLAB/SIMULINK using the multi-body dynamics solver Sim-Mechanics [43]. The simulations of the RM3 geometry performed by WEC-Sim has been directly compared to experimental data, demonstrating that the relative heave and pitch responses agree very well in terms of both amplitude and phase.

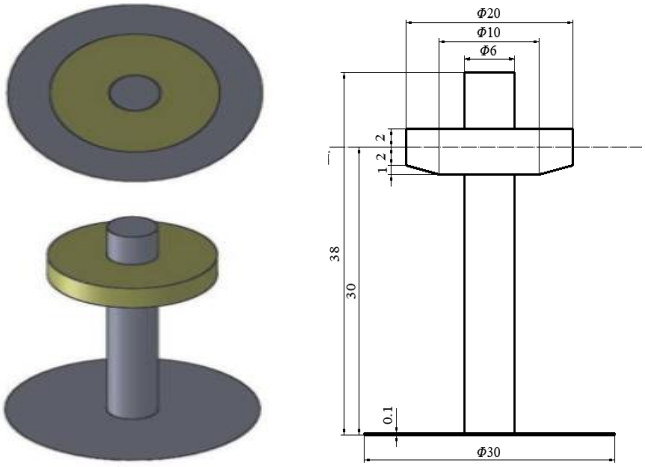

Fig. 4 Design parameters of the RM3 floating point absorber (Unit: m)

Table 2 Mass properties of dimensions for the RM3 WEC

Float								
Coordinates of the centre of gravity (m)		Mass (kg)	Moment of inertia I (kg·m^2)					
x	0.00	727010	I_{11}	2.09E+07	I_{12}	0.00E+00	I_{13}	0.00E+00
y	0.00		I_{21}	0.00E+00	I_{22}	2.13E+07	I_{23}	4.30E+03
z	-0.72		I_{31}	0.00E+00	I_{32}	4.30E+03	I_{33}	3.71E+07
Spar platform								
Coordinates of the centre of gravity (m)		Mass (kg)	Moment of inertia I (kg·m^2)					
x	0.0011	878300	I_{11}	9.44E+07	I_{12}	0.00E+00	I_{13}	0.00E+00
y	0.00		I_{21}	0.00E+00	I_{22}	9.44E+07	I_{23}	2.18E+05
z	-21.29		I_{31}	0.00E+00	I_{32}	2.18E+05	I_{33}	2.85E+07

The movement pattern of the WECs-breakwater hybrid system is similar to that of the RM3 system. Both supporting structures perform 6-DoF movements, and the WECs can only move in heave mode relative to the supporting structures. The difference between the systems is the number of WECs attached to the supporting structure. The number of WECs that can be calculated by the numerical model established in this paper can be changed from 1 to n. The curves of the present results were obtained by multiplying the WAFDUT result by a cosine function.

Fig. 5 shows the present results are in good agreement with the published WEC-Sim results by Ruehl et al. [29], with the maximum difference 3.0%. The overall agreement between the present results and the published WEC-Sim results verifies that the present model can accurately simulate

the multi-floating-body coupled constraint motion.

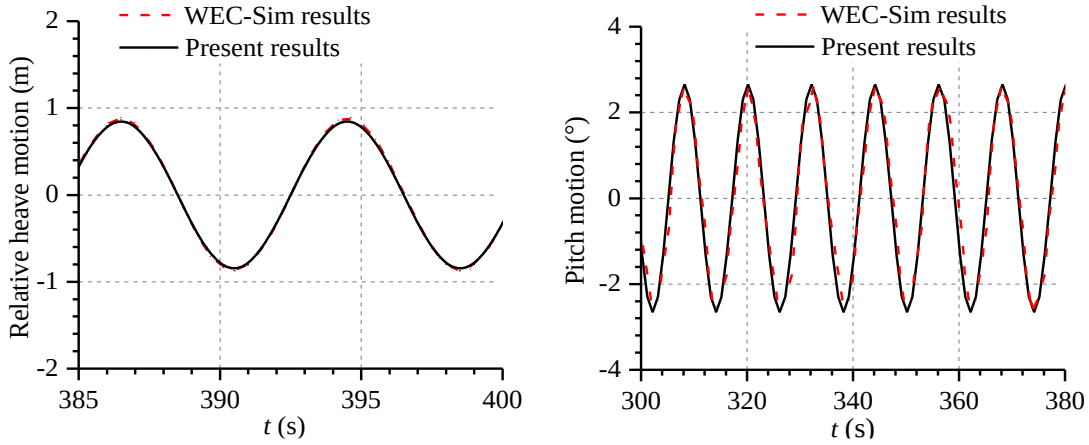

(a) Relative heave motion， b_{pto}=1200.0 kN·s/m, T=8.0 s (b) Pitch motion, b_{pto}=0.0 kN·s/m, T=12.0 s

Fig. 5 Comparison of the relative heave motion between the WEC and spar and surge motion between the present results and the published numerical results using WEC-Sim code

4 Results and discussions

4.1 Breakwater draft and width

The transmission wave amplitude A_t and focusing wave amplitude A_f of the floating breakwater with different drafts and widths were compared to optimize the size of the breakwater in this section. In practice, the breakwater width usually needs to be at least one-third of the target wavelength for satisfactory wave attenuation. Thus, the width of the breakwater was chosen as B=20.0 m for the average wave period of the target sea state 5.6 s with a wavelength λ=52.3 m. The length of the breakwater was assumed to be L=150.0 m. The motion of the breakwater will generate radiation potential which can enlarge the wave elevations, therefore to facilitate comparisons in this section the breakwater was assumed to be fixed.

Fig. 6 shows the transmission wave amplitude A_t and the focusing wave amplitude A_f of the breakwater with the draft D=10.0 m is relatively close to those of the breakwater with D=15.0 m in the period region 4.0 s <T< 8.0 s, representative of the most frequent waves of the target sea as shown in Table 1, with the difference by up to 8.83% and 1.99% respectively. This is because the velocities of water particles decay exponentially through the water depth, causing the effect of the breakwater draft on the transmission wave amplitude and the focusing wave amplitude to diminish when the draft extends sufficiently deep. The transmission wave amplitude of the breakwater with D=10.0 m is smaller than that of the breakwater with D=5.0 m when T> 6.6 s, but a little larger than that of the breakwater with D=5.0 m when 4.0 s <T< 6.6 s, with the difference by up to 28.0% and 15.5% respectively. This is because the diffraction potential on the lee side of the breakwater with D=10.0 m is larger than that with D=5.0 m and thus increases the wave elevations on the lee side of the breakwater with D=10.0 m, especially near the ends of the breakwater, as shown in Fig. 7. Fig. 7 only shows the wave elevations in the area of y> 0 m because the distribution of the wave elevations around the breakwater is symmetric about x axis. The When T > 6.6 s, the focusing wave amplitude of the breakwater with D=10.0 m is larger than that with D=5.0 m. These results demonstrate the wave attenuation and focusing performance of the breakwater with D=10.0 m is generally similar to that of the breakwater with D=15.0 m and is better than that of the breakwater with D=5.0 m.

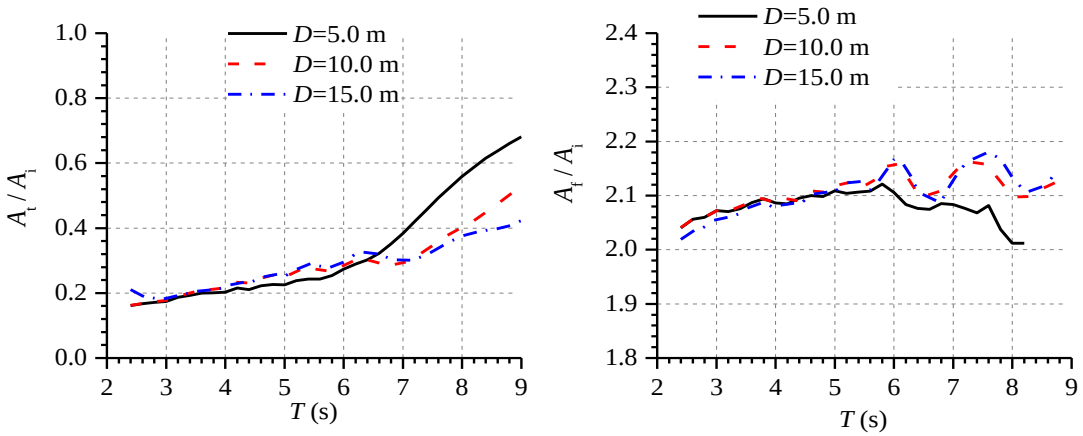

(a) Transmission wave amplitude (b) Focusing wave amplitude

Fig. 6 Variation of the transmission wave amplitude A_t (a) and focusing wave amplitude A_f (b) against wave period T for different breakwaters with width B=20.0 m

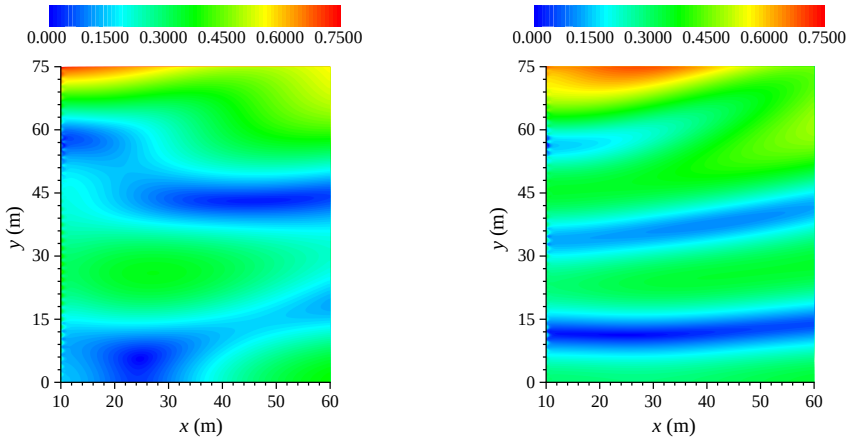

(a) D=5.0 m (b) D=10.0 m

Fig. 7 The distribution of the wave elevations on the lee side of the breakwater with different drafts D at T=5.4 s

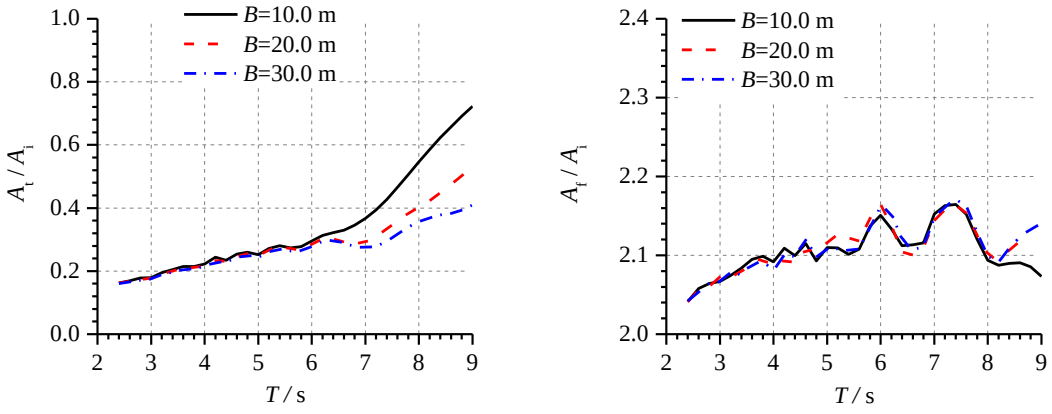

(a) Transmission wave amplitude (b) Focusing wave amplitude

Fig. 8 Variations of the transmission wave amplitude A_t and focusing wave amplitude A_f against wave period T for different breakwaters with draft D=10.0 m

Fig. 8 shows that the transmission wave amplitude decreases with increasing breakwater width, especially when T > 6.5 s. The focusing wave amplitude changes little with the increase of B in the period region 4.0 s <T< 8.0 s. The difference in transmission wave amplitude between the

breakwaters with B=20.0 m and B=30.0 m is smaller than that between the breakwaters with B=10.0 m and B=20.0 m, indicating the wave attenuation and focusing performance of the breakwater with B=20.0 m is close to that of the breakwater with B=30.0 m.

Balancing performance and the cost implications of breakwater size, the breakwater with draft D=10.0 m, width B=20.0 m and length L=150.0 m was selected to optimize the layout of the WEC in the next sections.

4.2 Effect of breakwater motion

The motion of the breakwater will generate radiation potential which can affect the wave attenuation and focusing performance of the breakwater. This section compared the transmission wave amplitudes and focusing wave amplitudes of the breakwater with different motion mode. The sizes of the breakwater were D=10.0 m, B=20.0 m and L=150.0 m.

Fig. 9 shows that the surge motion of the breakwater significantly increases both the transmission wave amplitude A_t and the focusing wave amplitude A_f. Compared with the fixed breakwater, A_t and A_f for the breakwater with surge motion increase by up to 214.9% at T=6.8 s and 20.6% at T=8.0 s respectively. The maximum transmission wave amplitude of the breakwater with surge motion is even larger than the incident wave amplitude when T> 8.0 s, which is because the effects of the radiation caused by the surge motion of the breakwater are quite large. The transmission wave amplitude and the focusing wave amplitude are little affected by the heave and pitch motions of the breakwater when 2.0 s<T< 5.0 s due to the very small amplitudes of the heave and pitch motions, as shown in Fig. 9 (c), and thus the radiation effects are weak. When T > 5.0 s, the heave motion amplitude rapidly increases, leading to enhanced radiation effects of the breakwater. Therefore, A_t and A_f significantly increase for breakwater with heave motion when T> 5.0 s, by up to 99.2% at T=8.2 s and 14.4% at T=9.0 s respectively. The pitch motion of the breakwater only slightly increases A_t and A_f when T> 5.0 s due to the small increase in pitch motion amplitude, only by up to 19.3% and 2.2% respectively.

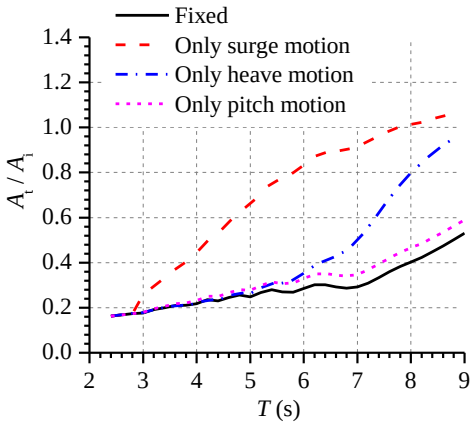

(a) Transmission wave amplitude

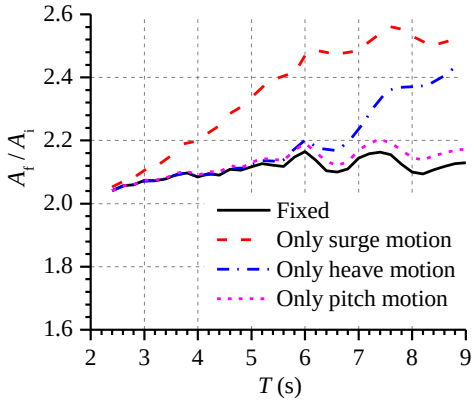

(b) Focusing wave amplitude

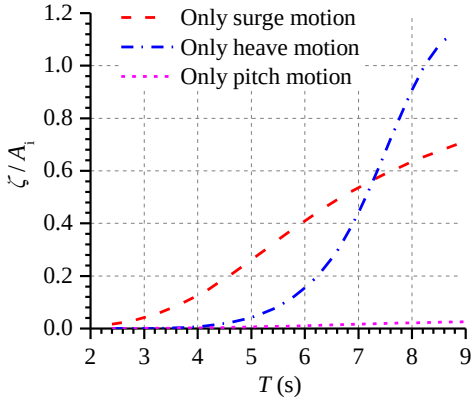

(c) Motion amplitude

Fig. 9 Variations of the transmission wave amplitude A_t, focusing wave amplitude A_f, and motion amplitude ζ against wave period T for breakwaters with different degrees of freedom

As the wave attenuation performance is of primary importance for the breakwater, the large increase in the transmission wave amplitude is unacceptable. Hence, the stiffness of the mooring system needs to be large enough to keep the surge and heave motions of the breakwater small. In this paper, the equivalent stiffness matrix of the mooring system is shown below:

$$\begin{bmatrix} 6.08e+08 & -2.90e-01 & -3.70e+00 & 3.60e+01 & -5.51e+09 & 1.65e+02 \\ 3.76e+00 & 3.01e+08 & -2.05e+00 & 2.95e+09 & -1.76e+01 & -2.24e+02 \\ -1.17e+00 & 1.45e-01 & 3.05e+08 & 2.50e+01 & -2.14e+01 & -1.08e+02 \\ -1.79e+00 & 2.95e+09 & -3.57e-01 & 1.08e+12 & -1.83e+01 & 1.86e+01 \\ -5.51e+09 & 1.43e-01 & -6.09e-01 & 9.49e+01 & 2.00e+12 & -4.70e+02 \\ 3.99e+00 & -2.80e-01 & -1.84e+00 & 6.09e+01 & -1.11e+01 & 3.42e+12 \end{bmatrix}$$

Fig. 10 shows the motions of the breakwater with mooring system decrease as expected. The transmission wave amplitude and the focusing wave amplitude both increase slightly compared to those of the fixed breakwater within acceptable limits, with the A_t increases by up to 19.9% and the A_f increases by up 1.6%. Therefore, the equivalent stiffness matrix is used in following sections.

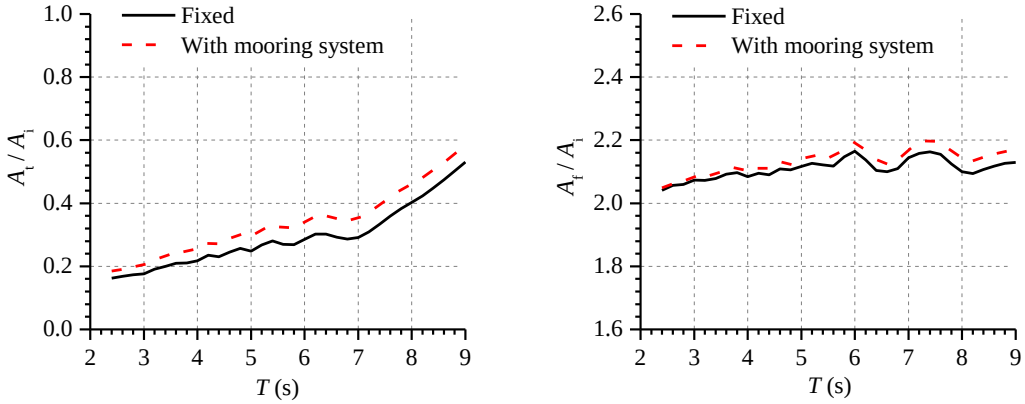

(a) Transmission wave amplitude

(b) Focusing wave amplitude

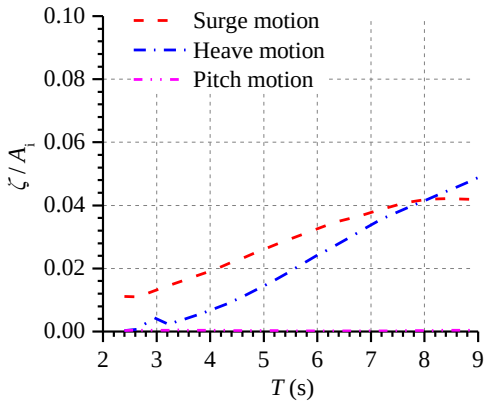

(c) Motion amplitude

Fig. 10 Variations of the transmission wave amplitude A_t, focusing wave amplitude A_f, and motion amplitude ζ against wave period T for breakwaters with mooring system

4.3 WEC Layout

To determine the optimal size of the WEC, five WECs with different ratios of width b to draft d were selected. The mass of these five WECs was kept constant, and the ratio of the breadth b to the length l was b/l=1.0. The detailed values of the dimensions of these five WECs are listed in Table 3. These five WECs were placed in front of a breakwater, with the distance between the WEC and the breakwater assumed to be 0.5 m. The breakwater parameters were constant with Section 4.2.

Table 3 Dimensions of the WECs with different b/d

b/d	b (m)	d (m)	l (m)
1	2.80	2.80	2.80
2	3.52	1.76	3.52
4	4.44	1.11	4.44
6	5.10	0.85	5.10
8	5.60	0.70	5.60

Fig. 11 (a) shows the total wave power per unit mass P_{ave} of the WEC becomes larger with b/d in the whole period region except when b/d=8. The P_{ave} of the WEC with b/d=8 is reduced in the low wave period region. Fig. 11 (b) presents the $W_{AEP/mass}$ increases when b/d gets bigger, and the rate of the increase gradually declines. Therefore, we can conclude that the WEC with larger b/d will extract more wave energy when in front of the breakwater. Considering the strength and fatigue problems of the WECs in practical engineering applications, the WEC with b/d=4 is chosen for this study.

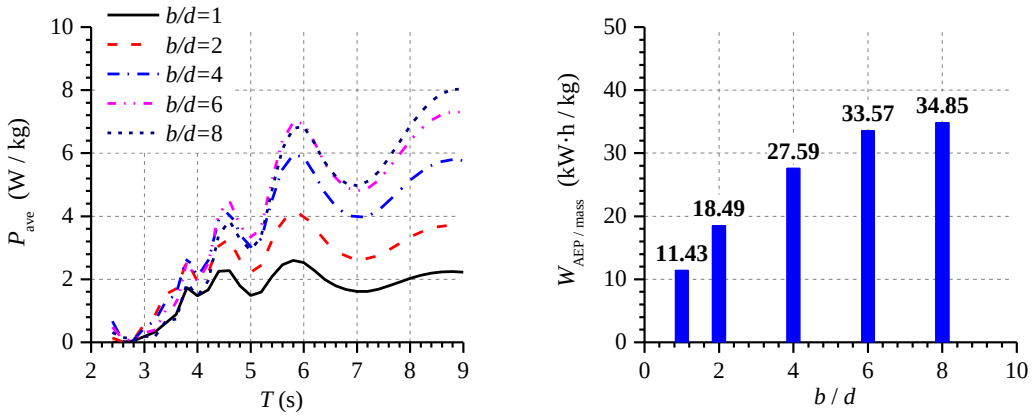

(a) Total wave power per unit mass (b) Annual energy production per unit mass

Fig. 11 Variations of P_{ave} and $W_{AEP/mass}$ of a WEC with different ratios of b/d in front of a breakwater against wave period T

Fig. 12 shows the spatial distribution of the wave elevations on the upward side of the breakwater at the average wave period T=5.6 s of the target sea state. We identify four wave focusing areas where the focusing wave amplitude A_f >2.0 m, labeled Area 1 to Area 4. The WEC with width b=4.44 m, length l=4.44 m, and draft d=1.11 m is placed in seven different positions, including the four wave focusing areas, to evaluate its wave extraction performance, as shown in Fig. 12.

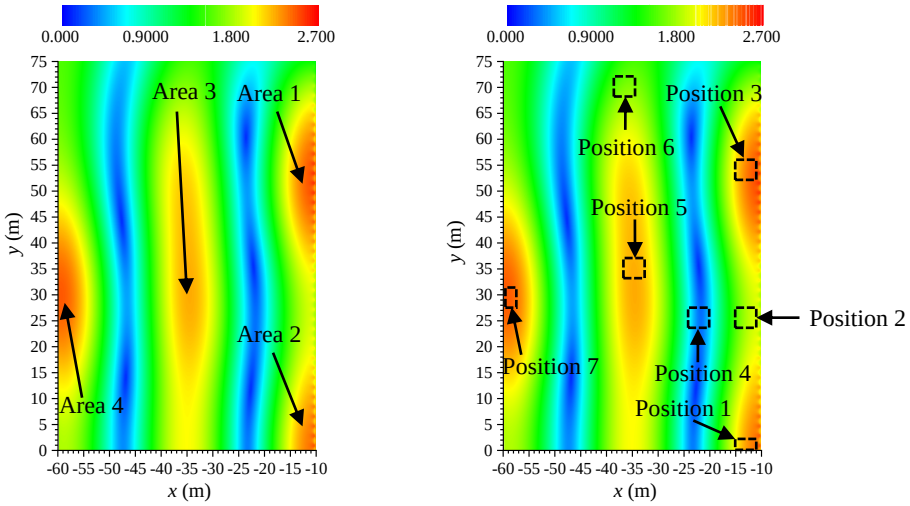

Fig. 12 The distribution of the wave elevations on the upward side of the breakwater at the average wave period T=5.6 s of the target sea state

The variation in total wave power P_{total} with wave period shown in Fig. 13 (a) shows that P_{total} minima occurs at certain wave periods, which is due to the change of the wave focusing amplitude A_f. Consider Position 5 as an example. Fig. 14 shows the wave focusing amplitudes A_f in Position 5 are quite small for T=4.6 s and T=7.6 s, causing the corresponding motion of the WEC sharply decrease, as shown in Fig. 13 (c). Similarly, the maximum P_{total} corresponds to larger wave focusing amplitude A_f. Fig. 13 (b) shows that W_{AEP} for WECs placed near the breakwater are similar and larger than those of the WEC placed further away from the breakwater corresponding to the larger minima of the P_{total} curves shown in Fig. 13 (a). This demonstrates the ideal layout of the WECs is near the breakwater, allowing the WECs to be beneficially installed on the

breakwater itself.

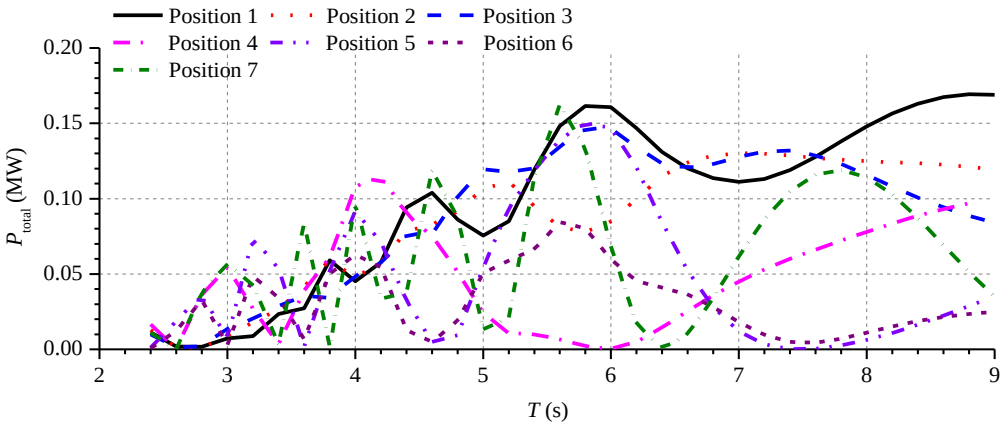

(a) Total wave power

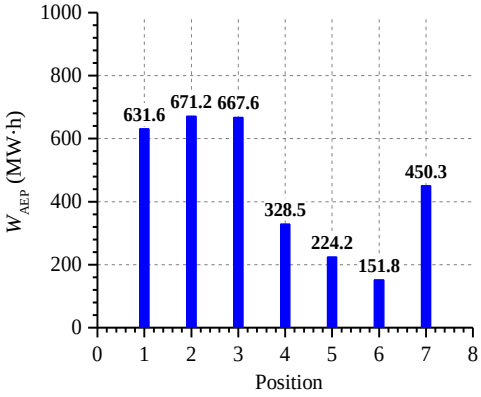

(b) Annual energy production

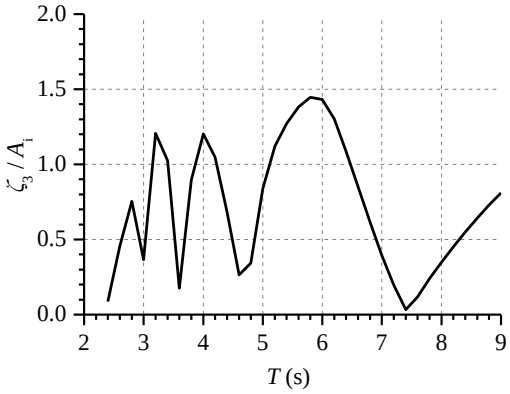

(c) Heave motion of the WEC placed in Position 5

Fig. 13 P_{total}, ζ_3, and W_{AEP} of the WEC in different positions

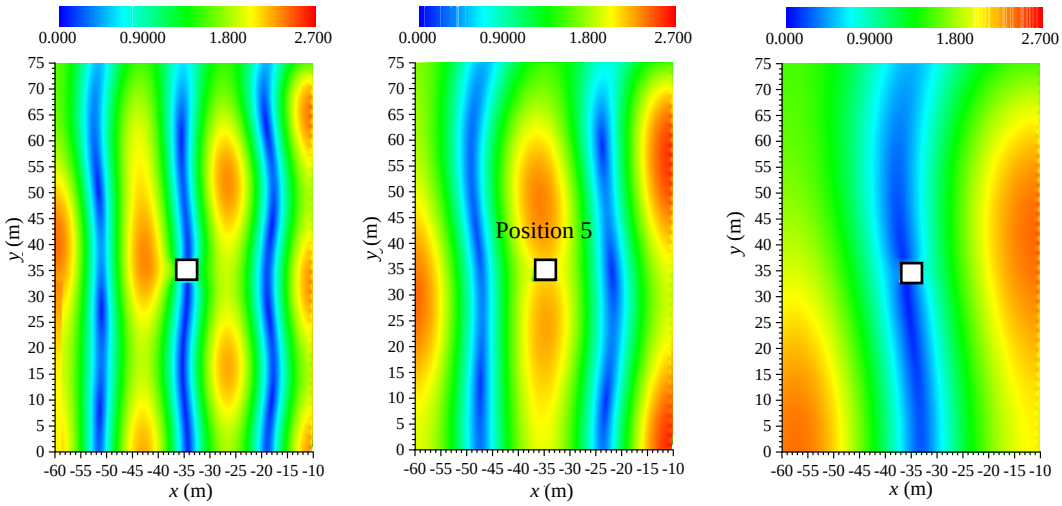

(a) T=4.6 s (b) T=5.6 s (c) T=7.6 s

Fig. 14 The distribution of the wave elevations on the upward side of the breakwater with a WEC placed in Position 5 at different wave periods

4.4 Number of devices in the WEC array

This section investigates the wave extraction performance of the WEC-breakwater system with

different numbers of devices n in the WEC array. Following the conclusions of Section 4.3, the WECs were placed spanning length L_1=132.0 m close to the breakwater with the distance between the WECs and breakwater B_g=0.50 m, as shown in Fig. 15. The WECs were numbered from negative to positive values, with number 0 being the central WEC. The widths and drafts of the WECs were kept as b=4.44 m and d=1.11m. The lengths of the WECs were l=10.16 m, 6.28 m, 4.55 m, 3.56 m, 2.94 m, 2.49 m for a total of n=7, 11, 15, 19, 23, 27 devices respectively. The separation distances B_l between WECs were equal to the length l of the WEC in each instance. The parameters of the breakwater were the same as in Section 4.2.

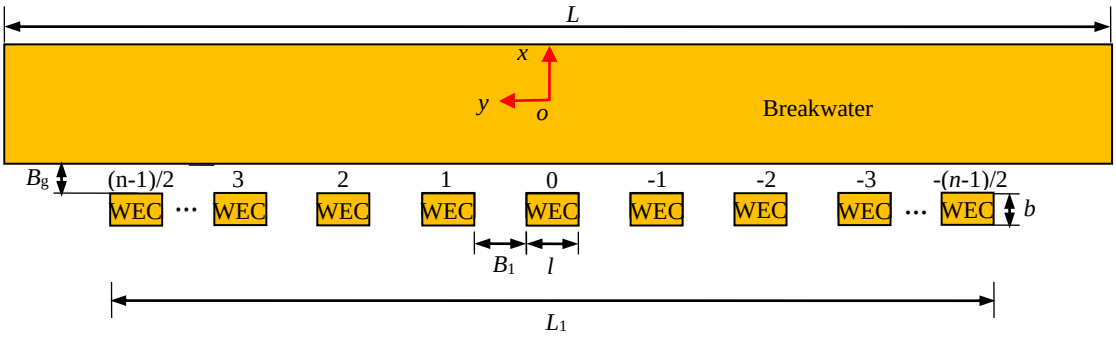

Fig. 15 A diagram of the placement of the WECs

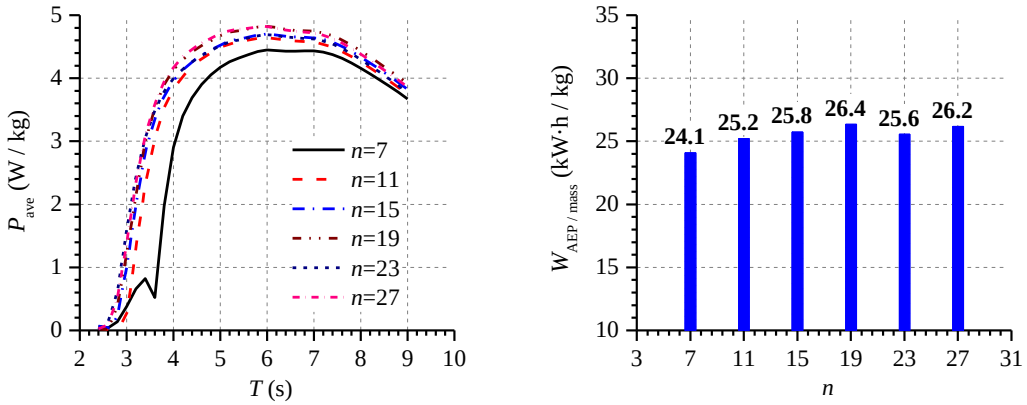

(a) Total wave power per unit mass

(b) Annual energy production per unit mass

Fig. 16 Variations of P_{ave} and $W_{AEP/mass}$ of the hybrid WEC-breakwater system with different number of WECs against wave period T

Fig. 16 shows that the total wave power per unit mass P_{ave} and the annual energy production per unit mass $W_{AEP/mass}$ are maximized for n=19. When n>19, the P_{ave} and the $W_{AEP/mass}$ of the WECs both reduce from that with n=19. The P_{ave} for longer wave periods is greater than that for small wave periods. This is because the wave focusing area close to the breakwater for long waves is wider than that for short waves as shown in Fig. 14, and thus the WECs are more likely to be in the wave focusing areas. When T>7.0 s, the P_{ave} reduces with further increases in the wave period T because the cross-array (y-direction) length of the wave focusing area and the wave elevation in the area near the breakwater gets smaller, as shown in Fig. 17. Fig. 18 shows how the $W_{AEP\text{-}i}$ of each WEC varies across the array, for n=19. The curve of the $W_{AEP\text{-}i}$ is symmetric about WEC 0, i.e. symmetric about x-axis. This is because the distribution of the wave elevations on the upward side of the breakwater is also symmetric about x-axis, leading to symmetric wave power of WECs about x-axis. The $W_{AEP\text{-}i}$ of WEC increases first and then drop off when WECs from center to the

ends of the breakwater. The $W_{AEP\text{-}i}$ of the 5 th and -5 th WECs both reach maximum values due to the highest probability of appearing in wave focusing area, as shown in Fig. 17.

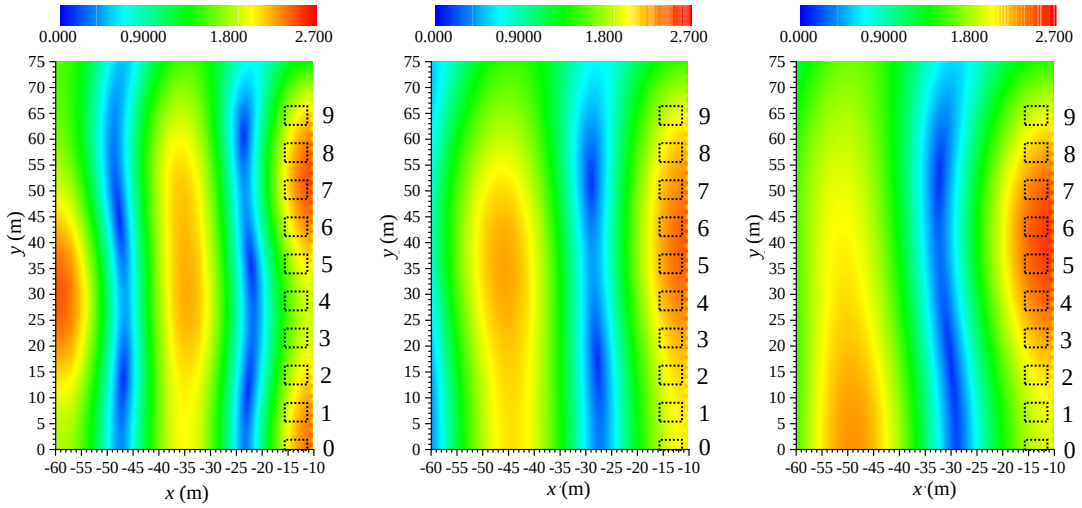

(a) T=5.6 s (b) T=6.6 s (c) T=7.0 s

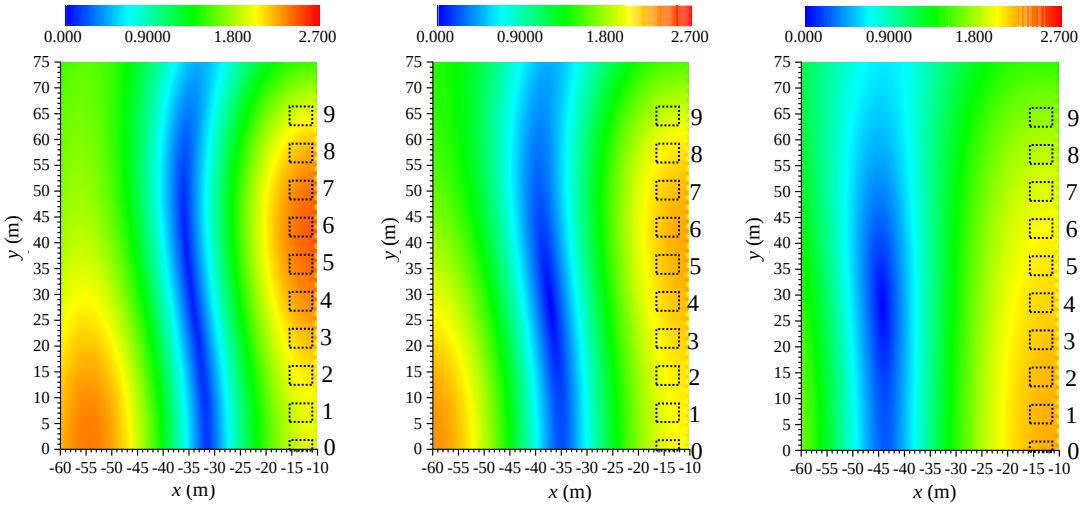

(a) T=7.6 s (b) T=8.0 s (c) T=8.6 s

Fig. 17 The distribution of the wave elevations on the upward side of the breakwater at different wave periods

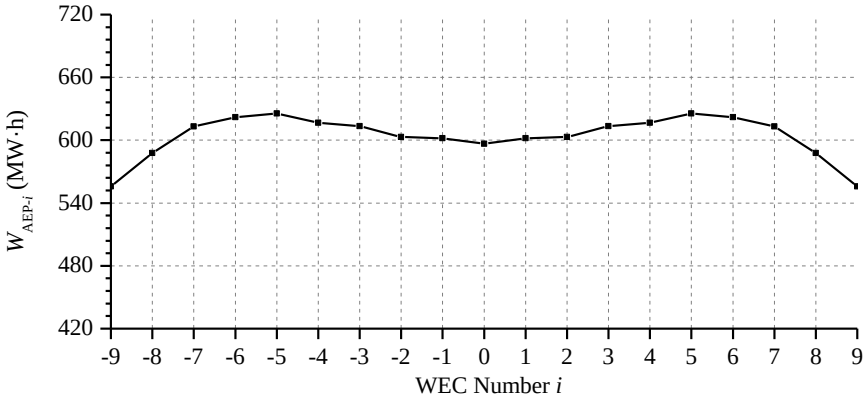

Fig. 18 Annual energy production W_{AEP} of each WEC with n=19

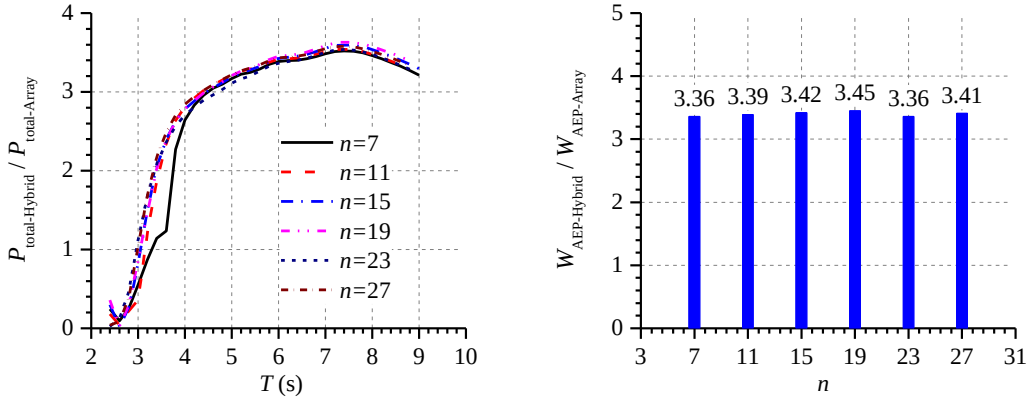

(a) Ratio of $P_{\text{total-Hybrid}}$ to $P_{\text{total-Array}}$ (b) Ratio of $W_{\text{AEP-Hybrid}}$ to $W_{\text{AEP-Array}}$

Fig. 19 Variations of the ratios of $P_{\text{total-Hybrid}}$, $W_{\text{AEP-Hybrid}}$ to $P_{\text{total-Array}}$, $W_{\text{AEP-Array}}$ with different number of WECs n

To study the effects of the breakwater on the wave extraction performance of the WECs, the total wave power and the annual energy production of the hybrid WEC-breakwater system ($P_{\text{total-Hybrid}}$ and $W_{\text{AEP-Hybrid}}$ respectively) were compared with those of an isolated WEC array without the presence of the breakwater ($P_{\text{total-Array}}$ and $W_{\text{AEP-Array}}$ respectively) for different numbers of WECs. It can be seen from Fig. 19 (a), the $P_{\text{total-Hybrid}}/P_{\text{total-Array}}$ is significantly higher than 1.0 for most wave periods, exceeding 3.0 when T > 4.4 s. Fig. 19 (b) shows that the ratio $W_{\text{AEP-Hybrid}}/W_{\text{AEP-Array}}$ is around 3.4 for all numbers of WECs and reaches a maximum value $W_{\text{AEP-Hybrid}}/W_{\text{AEP-Array}}$ =3.45 when n=19. This demonstrates that the wave focusing characteristic of the breakwater can improve the wave extraction performance of the WECs in front of the breakwater to a large extent, especially for longer waves. Therefore, integrating the WECs and breakwater is a promising approach to improve the energy extraction performance of the WECs.

4.5 WEC effect on the breakwater

To investigate the influence of the WECs on the breakwater, the heave and surge motion of the single breakwater and forces on the single breakwater were compared with those of the hybrid WEC-breakwater system in Fig. 20 and Fig. 21.

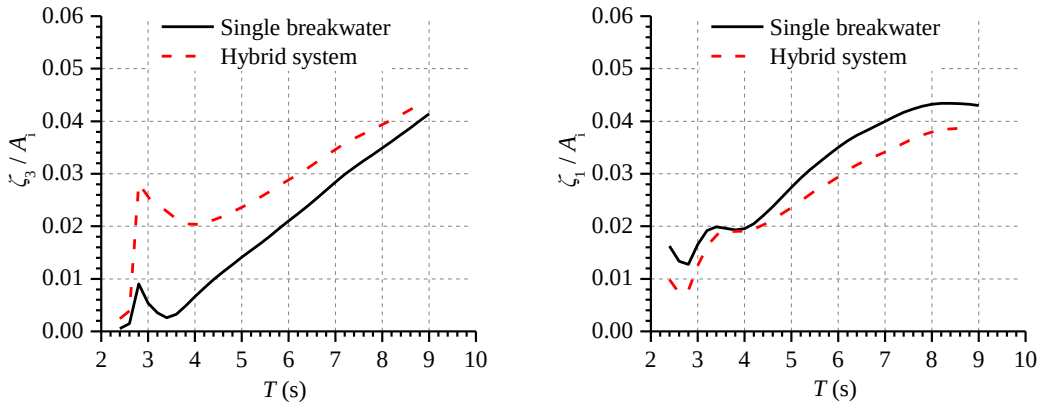

(a) Heave motion (b) Surge motion

Fig. 20 Comparison of the motion of the breakwater between the single breakwater and hybrid WECs-breakwater system

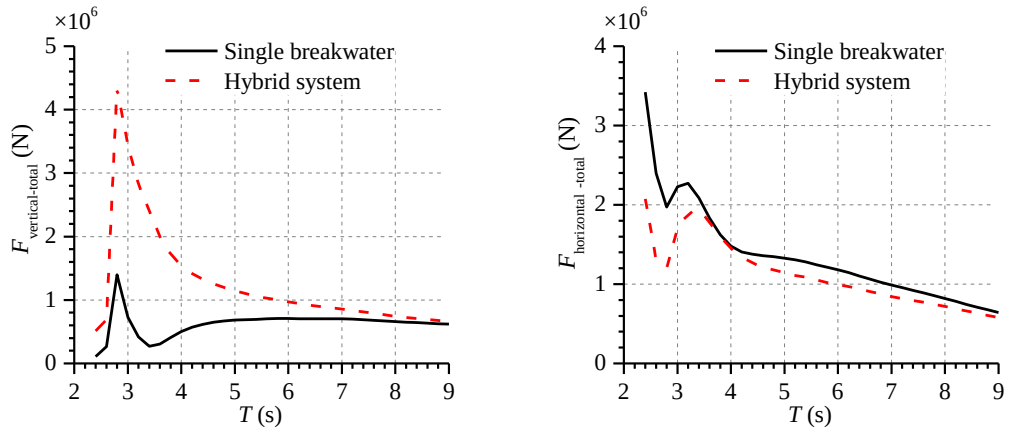

(a) Total vertical force (b) Total horizontal force

Fig. 21 Comparison of the total force on the breakwater between the single breakwater and hybrid WECs-breakwater system

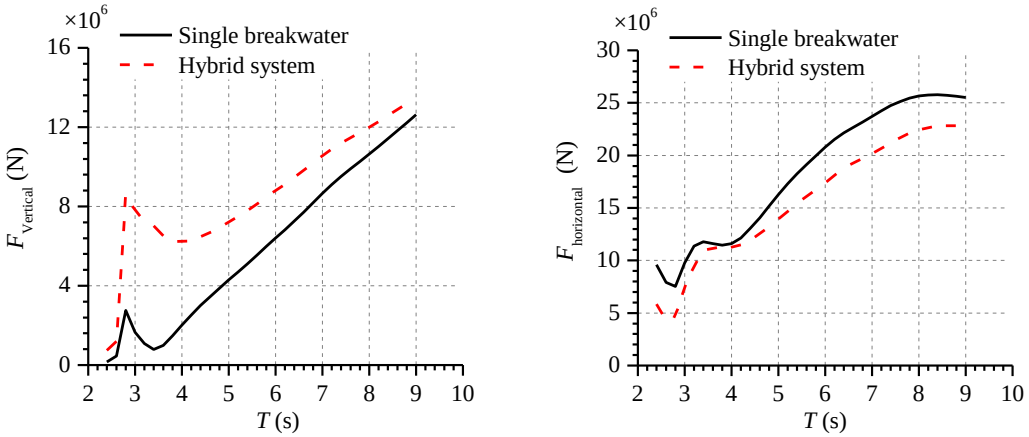

(a) Vertical stiffness force of mooring system (b) Horizontal stiffness force of mooring system

Fig. 22 Comparison of stiffness force of mooring on the breakwater between the single breakwater and hybrid WECs-breakwater system

The pitch motion of the breakwater was very small, so it was not shown in Fig. 20. In the hybrid system, the WECs cause the breakwater heave motion to increase and the surge motion to decrease. This is because the total vertical force acting on the breakwater is increased and the total surge force acting on the breakwater reduces due to the energy extraction of the WEC array, as shown in Fig. 21. The heave motion of the single breakwater peaks at T=2.8 s because that is the resonance period [13] [44] of the single breakwater. The resonance periods of WECs of the hybrid system are also T=2.8 s, so the heave motion of the breakwater of the hybrid system also peaks at this period. The probability of waves occurring at the resonance period is just 2.11%. Therefore, the rapid increase of the breakwater heave motion and the vertical stiffness force of the mooring system on the breakwater due to the resonance of the WECs and breakwater, are almost unlikely. As the wave period increases, the heave and surge motions of the single breakwater and the hybrid system breakwater both increase. The heave motion of the hybrid system breakwater reaches a maximum amplitude ζ_3 / A_i=0.044 at T=9.0 s, an increase of 6.88% compared to that of the single breakwater. For surge motion, the maximum amplitude ζ_1 / A_i=0.038 at T=9.0 s decreases by 10.2% compared to that of the single breakwater. The stiffness force of the mooring system is related to the motion of the breakwater, therefore, the vertical stiffness force on the breakwater of

the hybrid system is larger but the horizontal stiffness force is smaller than on the single breakwater, as shown in Fig. 22. The maximum horizontal stiffness force on the breakwater of the hybrid system is 2.28×10^7 N, 10.6% less than that on the single breakwater. However, the maximum vertical stiffness force of the hybrid system breakwater increases by 6.86% compared to the single breakwater. Consequently, the design requirements are higher for the mooring systems of the hybrid WEC-breakwater system.

4.6 Distance between the WECs and the breakwater

To study the effects of the gap distance B_g between the WECs and the breakwater on the performance of the WEC-breakwater system, five different distances B_g=1.0 m, 3.0 m, 5.0 m, 7.0 m, 9.0 m were simulated. Nineteen WECs were evaluated, and the dimensions of the WECs and the breakwater were the same as in previous sections.

Fig. 23 (a) shows the total wave power P_{total} for different gap distances between the WECs and the breakwater. We can see that the wave periods corresponding to the troughs of wave power shift from T=2.8 s to 5.4 s as the gap distance B_g increases. This is because the position of the area with the minimum wave elevations close to the breakwater moves from x=-13.0 m to x=-21.5 m when the wave period increases from 2.8 s to 5.4 s, which corresponds to the positions of the WECs as shown in Fig. 24. Similarly, the variation of the P_{total} peaks with wave period is also related to the change in position of the maximum wave elevation area close to the breakwater with wave period. The P_{total} of the WECs reduces with increasing e B_g for the most frequent wave periods 4.0 s <T< 8.0 s, leading to a reduction in the annual energy production of the WECs as shown in Fig. 23 (b). Thus, we conclude a smaller gap distance between the WEC array and the breakwater is beneficial for WEC performance, which is also preferable for practical engineering reasons.

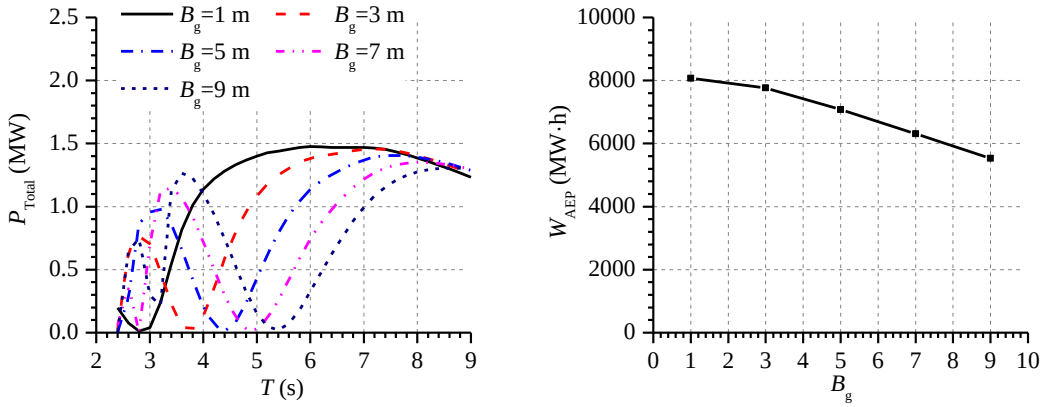

(a) Total wave power (b) Annual energy production

Fig. 23 Variations of the total wave power P_{total} and annual energy production W_{AEP} of the hybrid WEC-breakwater system with different gap distance B_g between the WECs and the breakwater

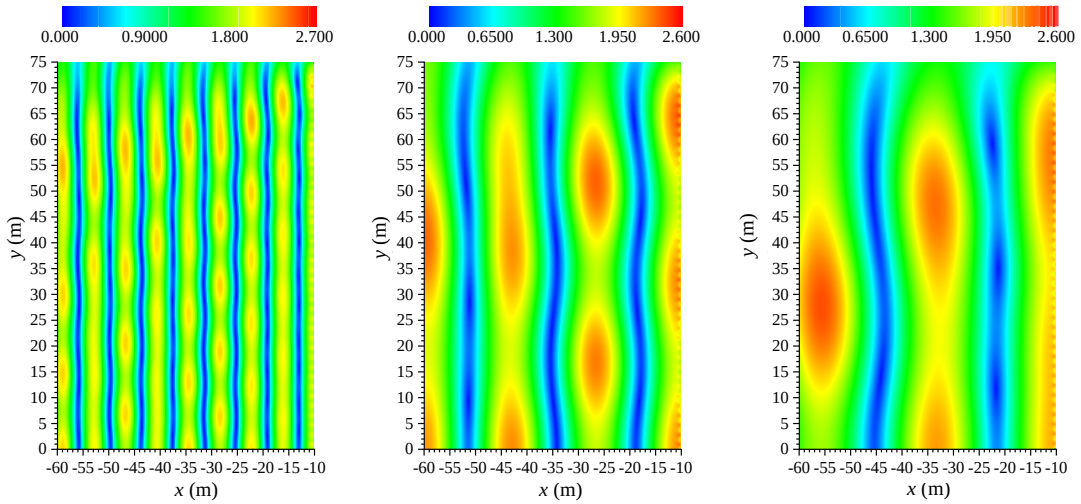

(a) T=2.8 s, B_g=1.0 m (b) T=4.4 s, B_g=5.0 m (c) T=5.4 s, B_g=9.0 m

Fig. 24 The distribution of the wave elevations on the upward side of the breakwater at different wave periods T and gap distance B_g.

5 Conclusions

In this paper, a method to optimize the hybrid system consisting of a wave energy converter array and a floating breakwater is developed based on the potential flow theory with viscous correction in frequency domain, focusing on analyzing the wave elevations around the floaters and the effects of the layout and number of the WECs on the wave energy extraction performance of the hybrid system. The following conclusions can be drawn from this study:

(1) Analyzing the wave elevations around the floaters is essential for optimizing the hybrid WEC-breakwater system. The wave elevation distribution clearly demonstrates the wave focusing and attenuation performance of the breakwater and provides a quick method to determine the optimal layout of the WECs.

(2) By analyzing the wave elevations in the lee side and upward side of the breakwater, we conclude that the breakwater with draft D=10.0 m, width B=20.0 m and length L=150.0 m satisfies the wave attenuation requirements of a sea area in South China Sea.

(3) The motion of the breakwater improves its wave focusing performance but reduces its wave attenuation performance. Compared with the fixed breakwater, the transmission wave amplitude A_t of the breakwater with surge motion increases by up to 214.9% at T=6.8 s. Therefore, a mooring system with large stiffness is necessary.

(4) WECs with a larger width-to-draft ratio will extract more wave energy when placed in front of the breakwater. The optimal layout of the WEC array is near the breakwater, and the optimal number of WECs n=19. The performance of the WECs was best for a small gap distance between the WEC array and the breakwater.

(5) For the hybrid WECs-breakwater system, the wave extraction performance of the WECs is improved due to the wave focusing performance of the breakwater, especially for longer wave periods. The annual energy production per unit mass of the WEC array of the hybrid system increases by up to 245.0% compared to the WEC array without a breakwater. The heave motion of the breakwater of the hybrid system increases due to the WECs, with the maximum amplitude increasing by 6.88% compared to a standalone breakwater. These results in the increase of the

vertical stiffness forces of the mooring system on the breakwater, with the maximum amplitude increasing by 6.86% compared to the single breakwater. However, the horizontal forces on the breakwater and the mooring system of the hybrid system decrease by 10.2% and 10.6% respectively.

Acknowledgements

This work was supported by the National Natural Science Foundation of China (52071096, 51979111). Student Research and Innovation Fund of the Fundamental Research Funds for the Central Universities (3072020GIP0105).

References

[1] Astariz S, Iglesias G. The economics of wave energy: A review. Renew Sustain Energy Rev 2015, 45:397–408.

[2] Mustapa MA, Yaakob OB, Ahmed YM. Wave energy device and breakwater integration: A review. Renew Sustain Energy Rev 2017, 77:43–58.

[3] Zhao XL, Ning DZ, Zou QP, Qiao DS, Cai SQ. Hybrid floating breakwater-WEC system: A review. Ocean Eng 2019, 186:106126.

[4] Wang RQ, Ning DZ. Dynamic analysis of wave action on an OWC wave energy converter under the influence of viscosity. Rene Energy 2020, 150: 578-588.

[5] Ning DZ, Zhou Y, Mayon R, Johanning L. Experimental investigation on the hydrodynamic performance of a cylindrical dual-chamber Oscillating Water Column device. Appl Energy 2020, 260:114252.

[6] Zhao XL, Du X, Li MW, Göteman M. Semi-analytical study on the hydrodynamic performance of an interconnected floating breakwater-WEC system in presence of the seawall. Appl Ocean Res 2021, 109:102555.

[7] Zhou Y, Ning DZ, Shi W, Johanning L, Liang DF. Hydrodynamic investigation on an OWC wave energy converter integrated into an offshore wind turbine monopole. Coast Eng 2020, 162:103731.

[8] Zheng SM, Zhang YL. Theoretical modeling of a new hybrid wave energy converter in regular waves. Rene Energy 2018, 128: 125-141.

[9] He F, Huang ZH, Law WK. An experimental study of a floating breakwater with asymmetric pneumatic chambers for wave energy extraction. Appl Energy 2013, 106(11): 222-231

[10] He F, Zhang HS, Zhao JJ, Zheng SM, Iglesias G. Hydrodynamic performance of a pile-supported OWC breakwater: An analytical study. Appl Ocean Res 2019, 88:326-340.

[11] Zheng SM, Zhang YL, Iglesias G. Coast/breakwater-integrated OWC: A theoretical model. Marine Struct 2019; 66:121-135.

[12] Xu CH, Huang ZH. A dual-functional wave-power plant for wave-energy extraction and shore protection: A wave-flume study. Appl Energy 2018, 229: 963-976.

[13] Zhang HM, Zhou BZ, Vogel C, Willden R, Zang J, Zhang L. Hydrodynamic performance of a floating breakwater as an oscillating-buoy type wave energy converter. Appl Energy 2020, 257: 113996.

[14] Madhi F, Sinclair ME, Yeung RW. The Berkeley Wedge: an asymmetrical Energy-Capturing floating breakwater of high performance. Marine Syst & Ocean Tech 2014, 9(1):05-16.

[15] Ning DZ, Zhao XL. Hydrodynamic performance of a pile-restrained WEC-type floating breakwater: An experimental study. Renew Energy 2016, 95: 531-541.

[16] Zhao XL, Ning DZ, Zhang CW, Kang HG. Hydrodynamic Investigation of an Oscillating Buoy Wave Energy Converter Integrated into a Pile-Restrained Floating Breakwater. Energies 2017, 10:712.

[17] Chen Q, Zang J. On the hydrodynamic performance of a vertical pile-restrained WEC-type floating breakwater. Renew Energy 2018, 146:414-425.

[18] Zhao XL, Ning DZ. Experimental investigation of breakwater-type WEC composed of both stationary and floating pontoons. Energy 2018, 155:226-233.

[19] Ning DZ, Zhao XL, Zhao M, Hann M, Kang HG. Analytical investigation of hydrodynamic performance of a dual pontoon WEC-type breakwater. Appl Ocean Res 2017, 65:102-111.

[20] Ning DZ, Zhao XL, Zhao M, Kang HG. Experimental investigation on hydrodynamic performance of a dual pontoon–power take-off type wave energy converter integrated with floating breakwaters. J Engineering for the Maritime Environment 2019, 233(4) 991–999.

[21] Zhang HM, Zhou BZ, Vogel C, Willden R, Zang J, Geng J. Hydrodynamic performance of a dual-floater hybrid system combining a floating breakwater and an oscillating-buoy type wave energy converter. Appl Energy 2020, 259: 114212.

[22] Zhang HM, Zhou BZ, Zang J, Vogel C, Fan TH, Chen CH. Effects of narrow gap wave resonance on a dual-floater WEC-breakwater hybrid system. Ocean Eng 2021, 225:108762.

[23] Zhao WH, Taylor PH, Wolgamot HA, Molin B, Taylor RE. Group dynamics and wave resonances in a narrow gap: modes and reduced group velocity. J Fluid Mech 2020, 883:A22-1

[24] Ning DZ, Zhao XL, Chen LF, Zhao M. Hydrodynamic performance of an array of wave energy converters integrated with a pontoon-type breakwater. Energies 2018, 11(3):685.

[25] Zhao XL, Ning DZ, Liang DF. Experimental investigation on hydrodynamic performance of a breakwater integrated WEC system. Ocean Eng 2019, 171:25-32.

[26] Cheng Y, Xi C, Dai SS, Ji CY, Cocard M, Yuan ZM, Incecik A. Performance characteristics and parametric analysis of a novel multi-purpose platform combining a moonpool-type floating breakwater and an array of wave energy converters. Appl Energy 2021, 292: 116888.

[27] Jin P, Zhou BZ, Malin G, Z.F. Chen ZF, Zhang L. Performance optimization of a coaxial-cylinder wave energy converter. Energy 2019, 174:450-459.

[28] Sun L, Taylor R E, Choo Y S. Responses of interconnected floating bodies. IESJ Part A. Civil & structural engineering, 2011, 4(3): 143-156

[29] Ruehl K, Michelen C, Kanner S. Preliminary verification and validation of WEC-Sim, An open-source wave energy conversion design tool. In: Proceedings of the ASME 2014 33rd International Conference on Ocean, Offshore and Arctic Engineering 2014, San Francisco, California USA.

[30] Zheng SM, Zhang YH, Zhang YL, Sheng WA. Numerical study on the dynamics of a two-raft wave energy conversion device. J. Fluids Struct 2015, 58: 271-290.

[31] Zheng SM, Zhang YL. Analysis for wave power capture capacity of two interconnected floats in regular waves. J. Fluids Struct 2017, 75:158–173.

[32] Zhang XT, Lu D, Guo F, Sun YG. The maximum wave energy conversion by two interconnected floaters: Effects of structural flexibility. Appl Ocean Res 2018, 71: 34-47.

[33] Sricharan VVS, Chandrasekaran S. Time-domain analysis of a bean-shaped multi-body floating wave energy converter with a hydraulic power take-off using WEC-Sim. Energy 2021, 223:119985.

[34] Ren JQ, Jin P, Liu YY, Zang J. Wave attenuation and focusing by a parabolic arc pontoon breakwater. Energy 2020, 217:119405.

[35] Duan JH, Cheng JS, Wang JP, Wang JQ. Wave diffraction on arc-shaped floating perforated breakwaters. China Ocean Eng 2012, 26(2):305-316.

[36] Chu YC, Cheng JS, Wang JQ, Li ZG, Jiang KB. Hydrodynamic performance of the arc-shaped bottom-mounted breakwater. China Ocean Eng 2014, 28(6): 749-760.

[37] Chang KH, Tsaur DH, Huang LH. Accurate solution to diffraction around a modified V-shaped breakwater. Coast Eng 2012, 68:56-66.

[38] Tay ZY. Performance and wave impact of an integrated multi-raft wave energy converter with floating breakwater for tropical climate. Ocean Eng 2020, 218:108136.

[39] Zhou BZ, Hu JJ, Sun K, Liu YY, Collu M. Motion response and energy conversion performance of a heaving point absorber wave energy converter. Front energy Res 2020, 8: 553295.

[40] Teng B, Taylor RE. New higher-order boundary element methods for wave diffraction/radiation. Appl Ocean Res 1995, 17: 71–77.

[41] Hu JJ, Zhou BZ, Vogel C, Liu P, et al. Optimal design and performance analysis of a hybrid system combing a floating wind platform and wave energy converters. Appl Energy 2020, 269:114998.

[42] Liu Y, Yoshida S, Hu C, Sueyoshi M, Sun L, Gao J, Cong P, He G. A reliable open-source package for performance evaluation of floating renewable energy systems in coastal and offshore regions. Energy Convers Manag 2018,174:516-536

[43] Yu YH, Lawson M, Ruehl K, Michelen C. Development and demonstration of the WEC-Sim wave energy conversion simulation tool. In: Proceedings of the 2nd Marine Energy Technology Symposium 2014, Seattle, WA.

[44] Chen ZF, Zhou BZ, Zhang L, Li C, Zang J, Zheng XB, Xu JA, Zhang WC. Experimental and numerical study on a novel dual-resonance wave energy converter with a built-in power take-off system. Energy 2018, 165:1008-1020.